ACCEPTED MANUSCRIPT • OPEN ACCESS

# Pure nanodiamonds for levitated optomechanics in vacuum

To cite this article before publication: Angelo C Frangeskou *et al* 2018 *New J. Phys.* in press https://doi.org/10.1088/1367-2630/aab700

# Pure nanodiamonds for levitated optomechanics in vacuum

**A C Frangeskou[1], A T M A Rahman[1,2], L Gines[3], S Mandal[3], O A Williams[3], P F Barker[2] and G W Morley[1]**

[1]Department of Physics, University of Warwick, Gibbet Hill Road, Coventry CV4 7AL, United Kingdom

[2]Department of Physics and Astronomy, University College London, Gower Street, London WC1E 6BT, United Kingdom

[3]School of Physics and Astronomy, Cardiff University, The Parade, Cardiff CF24 3AA, United Kingdom

E-mail: a.frangeskou@warwick.ac.uk, gavin.morley@warwick.ac.uk

**Abstract.** Optical trapping at high vacuum of a nanodiamond containing a nitrogen vacancy centre would provide a test bed for several new phenomena in fundamental physics. However, the nanodiamonds used so far have absorbed too much of the trapping light, heating them to destruction (above 800 K) except at pressures above ∼10 mbar where air molecules dissipate the excess heat. Here we show that milling diamond of 1000 times greater purity creates nanodiamonds that do not heat up even when the optical intensity is raised above 700 GW/m$^2$ below 5 mbar of pressure.

PACS numbers: 42.50.Wk, 65.80.-g, 03.75.-b, 05.40.Jc

*Keywords: optomechanics, optical tweezers, nanodiamond, nitrogen vacancy centres*

Submitted to: *New J. Phys.*

## 1. Introduction

Optically levitated nanodiamonds containing nitrogen vacancy ($NV^-$) center spin defects have been proposed as probes of quantum gravity [1, 2], mesoscopic wavefunction collapse [3–6], phonon mediated spin coupling [7], and the direct detection of dark matter [8, 9]. The $NV^-$ centre is a point defect in diamond that has a single electron spin which has long coherence times at room temperature and can be both polarized and read out optically [10, 11]. Progress with nanodiamonds levitated in optical dipole traps includes the detection of $NV^-$ fluorescence [12], optically detected magnetic resonance [13–15], and the observation of rotational vibration exceeding 1 MHz [16]. Nanodiamonds containing $NV^-$ centers have been trapped using ion traps at atmospheric pressure [17, 18] and in vacuum [19], and a magneto-gravitational trap has allowed nanodiamond clusters to be held below $10^{-2}$ mbar [20]. However, the latter design requires permanent magnets for the levitation, which is incompatible with the trap-and-release experiments [1, 2, 6] that reach large distance spatial superpositions of the centre-of-mass as desired for all of the fundamental physics experiments mentioned above.

A key requirement of the aforementioned proposals is that the nanodiamonds are levitated in high vacuum to prevent motional decoherence arising from gas collisions. However, nanodiamond has been reported to heat up and eventually burn or graphitize below ∼20 mbar due to the absorption of trapping light by defects and impurities prevalent in the commercially available nanodiamonds used thus far [13, 14, 21]. Even in experiments where the trapping potential is formed by something other than an optical field, substantial laser induced heating has been reported at moderate pressures because of the laser light required to excite $NV^-$ centres [19]. Heating not only eventually destroys the nanodiamond, but has been shown to be detrimental to the fluorescence intensity of the $NV^-$ centre, which is necessary for the optical read out of the spin state [22]. With non-levitated nanodiamonds, reducing the electron spin concentration has been shown to drastically improve spin coherence times of $NV^-$ centres [23, 24]. We also note that heating is a problem more generally in optical trapping and not unique to nanodiamond [25, 26].

Here we report on levitated nanodiamonds milled from pure low nitrogen chemical vapour deposition (CVD) grown bulk diamond. Whilst methods such as reactive ion etching of diamond to form nano-pillars are known to produce superior quality nanodiamonds compared to milling [24], milling is the only technique we are aware of that produces large enough quantities of nanodiamonds for the common nanoparticle injection methods employed in optomechanics. Our previous study had shown that commercial nanodiamonds (Adámas Nanotechnologies) milled from impure high-pressure high-temperature (HPHT) diamond can reach temperatures in excess of 800 K at 20 mbar, enough to burn or graphitize the nanodiamond [21]. In bulk diamond, the source of infrared absorption is known to be extrinsic [27–29]. It has been suggested that the source of heating was absorption of the trapping light by amorphous carbon on the surface of the nanodiamond and defects within the diamond [21]. Our milled

CVD nanodiamonds, which are 1000 times purer, remain at room temperature at lower pressures than the pressures attainable with commercially available material. These results show that impurities inside the nanodiamond are the dominant source of unwanted absorption and heating in commercially available nanodiamonds. We observe nanodiamonds to be suddenly ejected from the trap below 4 mbar (typically at $\sim 1$ mbar), which we attribute to previously observed trapping instabilities at intermediate vacuum that can be overcome with active damping (feedback cooling) of the centre-of-mass motion [30–32].

## 2. Theory

An optical dipole trap (optical tweezers) is formed by a focussed laser beam as shown in figure 1 (a). A sub-wavelength sized dielectric particle satisfies the Rayleigh scattering criterion and can be approximated as a point dipole, and in the limit of small oscillations [33] and the paraxial approximation [34], the trap potential is harmonic with a spring constant

$$k_{trap} = 4\pi^3 \frac{\alpha P}{c\varepsilon_0} \frac{(\text{N.A.})^4}{\lambda^4}, \tag{1}$$

where $\alpha$ is the polarizability of the particle, $P$ is the optical power, N.A. is the numerical aperture of the trapping lens, $c$ is the speed of light, $\varepsilon_0$ is the vacuum permittivity, and $\lambda$ is the trapping laser wavelength [32]. Whilst the trap forms a harmonic potential, collisions with the surrounding gas induce Brownian dynamics as seen in figure 1(b), and the motion of the particle is therefore governed by

$$m\ddot{x}(t) + m\Gamma_0\dot{x}(t) + m\omega_0^2 x(t) = f_B(t), \tag{2}$$

where $x(t)$ is the time dependent position along the $x$ axis (transverse to the optical axis), $m$ is the mass, $\Gamma_0$ is the damping rate, $\omega_0 = \sqrt{k_{trap}/m}$, and $f_B(t)$ is a Gaussian random force with $\langle f_B(t)\rangle = 0$ and $\langle f_B(t) f_B(t-t')\rangle = 2m\Gamma_0 k_B T_{cm}\delta(t-t')$, where $T_{cm}$ is the centre-of-mass temperature. Similar equations may be written for the $y$ (transverse) and $z$ (along the optical axis) directions. It can then be shown that the power spectral density is [33]

$$S_{xx}(\omega) = \frac{2k_B T_{cm}}{m} \frac{\Gamma_0}{(\omega^2 - \omega_0^2)^2 + \omega^2\Gamma_0^2}. \tag{3}$$

We fit the experimental data with (3), from which we may extract the nanodiamond's centre-of-mass temperature, damping rate, size, and mechanical frequency.

The centre-of-mass and internal temperatures are linked by $T_{cm} = (T_{imp}\Gamma_{imp} + T_{em}\Gamma_{em})/(\Gamma_{imp} + \Gamma_{em})$, where the subscripts *imp* and *em* denote the temperature and damping coefficients of impinging and emerging gas molecules, respectively [26]. Gas molecules thermalize with the nanodiamond, and the temperature of the nanoparticle is then $\alpha_g T = T_{em}$, where $0 \leq \alpha_g \leq 1$ is the thermal accommodation coefficient which determines the degree of thermalization [26]. By measuring the centre-of-mass temperature of levitated Rayleigh particles as a function of trapping power, $P$, one may deduce whether the nanodiamond is heating or at room temperature.

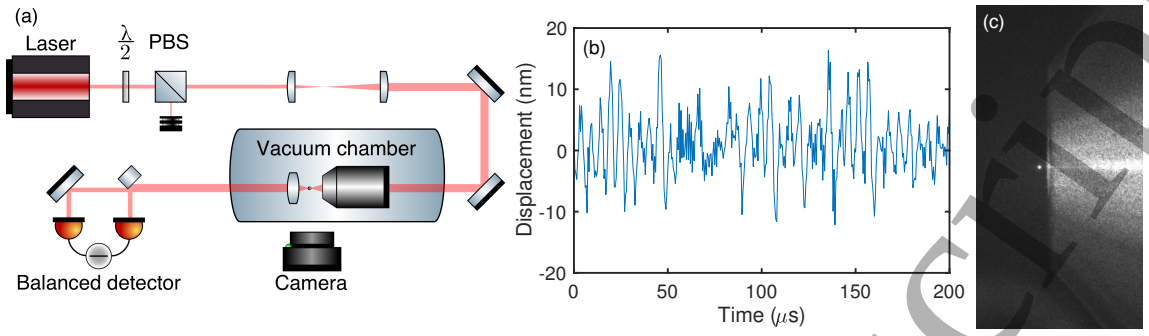


**Figure 1.** (a) Schematic of the experimental setup. A half-wave plate ($\lambda/2$) and polarizing beamsplitter (PBS) control the power of the laser. A microscope objective housed inside a vacuum chamber focusses the beam to form the dipole trap. Unscattered and scattered light from trapped nanodiamonds is collimated by an aspheric lens and sent to a balanced detector using one half-mirror and one full mirror. A CMOS camera monitors scattering intensity from above the vacuum chamber. (b) Calibrated time domain signal from the balanced detector, taken with a nanodiamond trapped at 4 mbar undergoing harmonic and Brownian dynamics. (c) Photograph of a levitated nanodiamond (white spot, left) trapped at the focus of the objective (right).

## 3. Methods

The starting material for the nanodiamonds was 150 mg of bulk CVD diamonds (Element Six 145-500-0274-01). Electron paramagnetic resonance (EPR) allows for the quantification of spin concentrations by comparing the EPR spectrum to the spectrum of a reference sample, in this case a CVD diamond with a known concentration (41 ppb) of single substitutional nitrogen ($N_s^0$). Rapid passage EPR was used for an enhanced signal-to-noise ratio and reduced acquisition time [35]. Twenty bulk samples of the same grade material were measured in a Bruker X-band EMX spectrometer. EPR spectra are shown in figure 2 (a). The [100] axis of each sample was aligned to the magnetic field so that all possible orientations of $N_s^0$ were equivalent with respect to the magnetic field. The field was swept from 338 to 358 mT in 10 s to satisfy the rapid passage condition. The concentration of $N_s^0$ in the twenty bulk samples averaged (121 ppb), varying from (95 ppb) to (162 ppb). This signifies an increase in purity of approximately three orders of magnitude compared to the 150 ppm HPHT synthesized starting material used to make the nanodiamonds used for previous work [12–21].

The diamonds were converted into nanodiamonds using silicon nitride ball milling and then purified with phosphoric acid at 180°C and sodium hydroxide at 150°C to remove the milling material, followed by a 5 hour 600°C air anneal. 532 nm Raman spectroscopy revealed no detectable contamination of silicon nitride as shown in figure 2 (c). These surface treatments target a similar surface termination as commercially supplied fluorescent nanodiamonds [36]; while there may be small differences, we believe they are not significant as the surface is partially burned away as shown in figure 2 (d).

The optical dipole trap shown in figure 1 (a) was formed by focussing a single longitudinal mode 1064 nm Nd:YAG laser (Elforlight I4-700) with a microscope

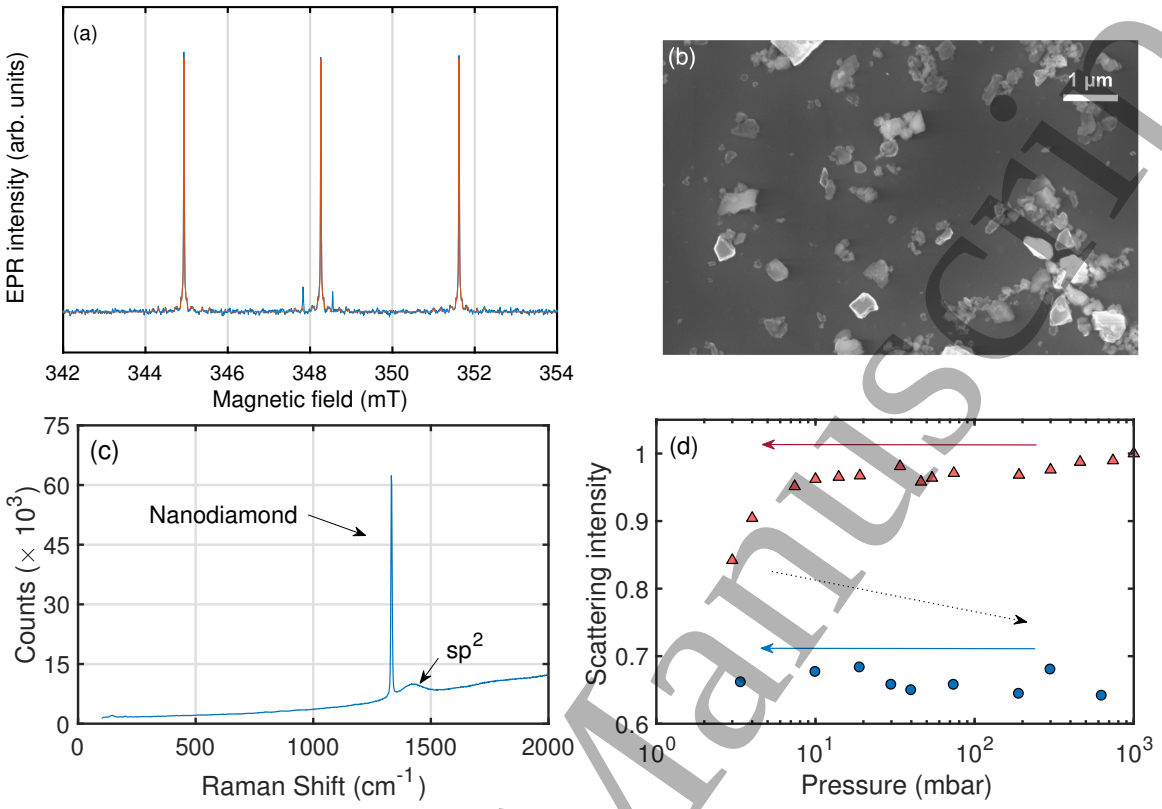


**Figure 2.** (a) Rapid passage EPR spectrum of the single substitutional nitrogen defect in diamond. The orange line is the fit to the data (blue). The defect has electron spin $S = 1/2$ and nuclear spin $I = 1$, resulting in a central line and two hyperfine lines corresponding to the nuclear spin manifolds. The substitutional nitrogen concentration is deduced from the spectrum. (b) SEM image of the nanodiamonds after ultrasonication. (c) 532 nm Raman spectrum of the nanodiamonds showing a diamond peak at 1332 $cm^{-1}$, an amorphous ($sp^2$) carbon peak at $\approx$ 1400 $cm^{-1}$ and no detectable SiN. The broad baseline and other small features are from the alumina substrate. The exposure time used was 10 s. (d) Scattering intensity of a single nanodiamond as the pressure is reduced from atmospheric to 4 mbar (red triangles). The chamber is then vented back to atmospheric pressure (black dotted arrow) and evacuated for a second time (blue points). Minimum trapping power is used on the second evacuation, with the scattering intensity recorded after measurements to verify that the size of the nanodiamond has not changed during power variation. The scattering intensity is normalised to the intensity at atmospheric pressure when the nanoparticle is initially trapped.

objective (Nikon N.A. 0.95) housed inside a vacuum chamber. The power of the laser was controlled with a half-wave plate and polarizing beam-splitter, which transmits horizontally polarized light to the objective lens. Un-scattered and scattered light from the trapped nanodiamond was collimated by an aspheric lens and sent to an InGaAs balanced detector which monitors the $x$ motion in an interferometric scheme described in [32, 37]. Our position sensitivity of 10 pm/$\sqrt{\text{Hz}}$ allows us to see the harmonic and Brownian dynamics of nanoparticles as shown in figure 1 (b).

The nanodiamonds were suspended in pure methanol and sonicated prior to

trapping. Figure 2 (b) shows a scanning electron micrograph of the nanodiamonds after sonication. Nanodiamonds were trapped by dispersing them into the vacuum chamber at atmospheric pressure using a nebulizer. Constancy of mass is a requirement of the power spectral density analysis, therefore nanodiamonds were first taken to ∼3-4 mbar using the maximum available trapping power to remove surface contaminants [21], and then brought back to atmospheric pressure after a minimum of one hour at vacuum. Scattered light from the nanodiamond was monitored with a CMOS camera above the vacuum chamber to ensure the size remained constant across all centre-of-mass measurements. Figure 2 (d) shows that the scattering intensity falls by 10-20% after the initial evacuation due to the removal of surface contaminants, and then remains constant on the second evacuation when measurements were made [21].

The live position signal from the balanced detector was recorded with a high resolution PC oscilloscope. After normalising by the power, the data is Fourier transformed to reveal the power spectral density and fit with $S_{xx}(\omega)$ as shown in figure 3 (a). The fitting parameter $A = 2C^2 k_B T_{cm}/m$ was extracted for different powers at a fixed pressure of 4 mbar, where $C$ is a calibration constant for converting from the detector signal in volts to meters. The dependence of $A$ upon the laser power for a fixed mass determines whether or not the nanodiamonds were heating. The centre-of-mass temperature was measured as a function of power rather than pressure to take advantage of the increased signal-to-noise at low pressure. The centre-of-mass temperature was inferred from $A$ by measuring $A$ at a higher pressure $p_1$ where the nanodiamond is confirmed to be at room temperature, and then $T_{cm_2} = T_{cm_1}(A_{p_2}/A_{p_1})$, where $T_{cm_1} = 298$ K, and $A_{p_1}$ and $A_{p_2}$ are the values of $A$ at high pressure $p_1$ and low pressure $p_2$, respectively. Errors were determined by taking the standard deviation of repeated measurements of a single data point, and summing it with the fitting error.

## 4. Results

Representative data of the nanodiamonds studied in this article are presented in figure 3. A linear fit of the data in figure 3 (b) gives a heating rate of 24±230 K/W, demonstrating that the centre-of-mass temperature does not depend on the trapping laser power even as it was more than doubled up to approximately 300 mW, corresponding to an intensity at the focus of ∼750 GW/m$^2$. This shows that by absorbing less trapping light, the nanodiamonds are able to dissipate any excess heat. Furthermore, we were able to keep most nanodiamonds trapped at ∼ 3-4 mbar for over a week with the maximum available trapping power. Below this pressure, nanodiamonds were susceptible to sudden ejection from the trap due to trapping instabilities [30].

The average heating rate for all but one of the nanodiamonds studied was $27 \pm 190$ K/W, ranging from -27 K/W to 164 K/W, none of which exhibited heating above the margin of error. One particle, however, was observed to heat. In cases where the c.m. temperature is raised above thermal equilibrium, the model described in [26] can be used to deduce the internal temperature, which was inferred to be 600 K at maximum power

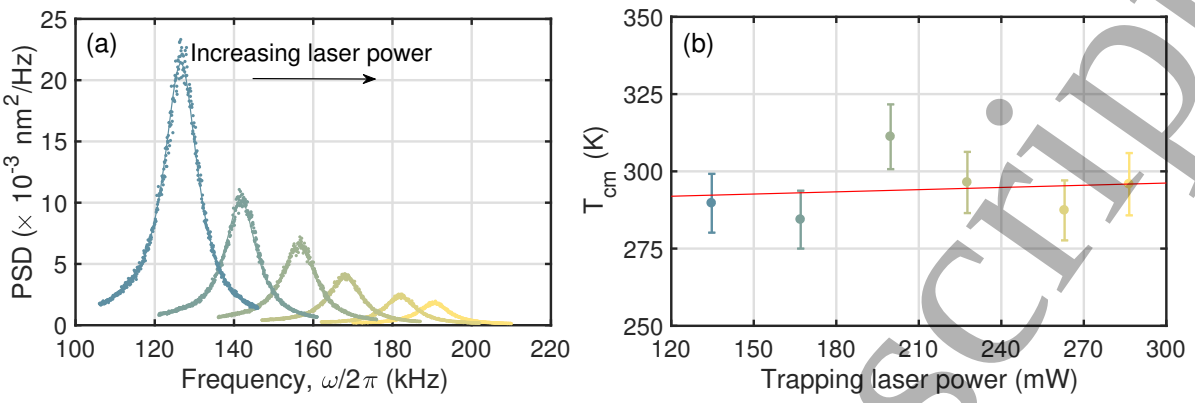


**Figure 3.** (a) Experimentally measured power spectral densities (· · · · · ·) of a single trapped nanodiamond at 4 mbar as trapping power is increased from 130 to 290 mW (left to right), fit with (3) (——). As expected from (1), the trap frequency increases as $\omega_0 \sim \sqrt{P}$. From the fit, we determine the radius of the nanodiamond to be $r \approx 36$ nm (equivalent sphere). (b) Corresponding centre-of-mass temperatures of the same nanodiamond, showing no dependence on the trapping laser power.

for the diamond that showed heating above the margin of error. Possible explanations for the heating could be the presence of surface contaminants, or graphitic carbon trapped within a grain boundary in the nanodiamond or between boundaries in a cluster of nanodiamonds.

## 5. Discussion

The upper-bound absorption coefficient at 1064 nm of the parent material used to make our nanodiamonds is 0.03 $cm^{-1}$ [28]. This is slightly lower than the absorption coefficient of high purity silica (0.11 $cm^{-1}$) [38], a material that has already been optically trapped in high vacuum in numerous studies [30–32, 39–41]. Therefore, if the motion of the nanodiamond can be damped through the period of intermediate vacuum, it may be possible to take the nanodiamonds to high vacuum where proposals [1–9] could be realised. It is worth noting that single crystal CVD diamonds that are two orders of magnitude purer than the nanodiamonds used here are commercially available.

In order to predict an upper-bound to the minimum pressure our nanodiamonds can reach, we utilise a thermodynamic model based on two heat dissipation mechanisms: gas cooling and blackbody radiation. Equation (4) models a sub-wavelength sphere with an absorption cross-section related to the complex permittivity of the sphere, heat dissipation due to gas molecule collisions, and the dissipation of blackbody radiation.

The total heating rate of the sphere is then expressed as [42–44]

$$\frac{\partial q}{\partial t} = \underbrace{3IkV\left(\mathrm{Im}\frac{\epsilon-1}{\epsilon+2}\right)}_{\text{Absorption}} - \underbrace{\frac{\alpha_g}{2}\pi r^2 \bar{v} p \frac{\gamma+1}{\gamma-1}\left(\frac{T}{T_0}-1\right)}_{\text{Gas}} \quad (4)$$
$$- \underbrace{\frac{72\zeta(5)V}{\pi^2 c^3 \hbar^4}\left(\mathrm{Im}\frac{\epsilon_{bb}-1}{\epsilon_{bb}+2}\right)k_B^5 T^5}_{\text{Black-body}},$$

where $I$ is the trapping laser intensity, $k = 2\pi/\lambda$, $V$ is the nanoparticle volume, $\epsilon = \epsilon' + i\epsilon''$ is the complex permittivity, where $\epsilon'$ is equal to 5.8 for diamond and 2 for silica, and $\epsilon'' = (\lambda\mu/4\pi)^2$ where $\mu$ is the absorption coefficient with units of $\mathrm{m}^{-1}$. $\alpha_g$ is a phenomenological thermal accommodation coefficient (taken as 1 for diamond, and 0.777 for silica [26]), $r$ is the nanoparticle radius, $\bar{v} = \sqrt{8k_B T_0/\pi m_{\mathrm{gas}}} \approx 500\ \mathrm{ms}^{-1}$ is the mean gas speed, $T_0 = 298$ K is the gas temperature, $m_{\mathrm{gas}} \approx 4 \times 10^{-26}$ kg is the mass of a gas molecule, $p$ is the gas pressure, $\gamma = 7/5$ is the gas specific heat ratio, $\zeta(5) = 1.04$ is the Riemann zeta function, and $\hbar$ is the reduced Planck's constant. $\mathrm{Im}\frac{\epsilon_{bb}-1}{\epsilon_{bb}+2} \approx 0.1$ is assumed for silica [38, 44], and $\approx 10^{-3}$ for diamond [45, 46], approximately corresponding to the average permittivities around blackbody wavelengths at $T \approx 1000$ K.

We model the steady state temperatures as a function of pressure for 25 nm radius nanodiamonds (the average size of the nanodiamonds used in this study) using upper-bounds of the absorption coefficients measured in [28, 29] by laser calorimetry. Assuming a linear relationship between defect concentration and absorption coefficient [47], we may also model diamonds for which the absorption coefficient is below the detection limit of laser calorimetry ($0.001\ \mathrm{cm}^{-1}$ for a 1 mm thick sample [29]). Figure 4 shows the predicted temperature as a function of pressure for nanodiamonds of various absorption coefficients.

With the exception of the commercial nanodiamonds used in [12–21], no significant heating is expected above 1 mbar, as confirmed by our experimental results. Above this pressure, the surrounding gas efficiently dissipates the heat generated by absorption of the trapping laser. At approximately $10^{-2}$ to $10^{-3}$ mbar, blackbody radiation becomes the dominant heat dissipation mechanism and the temperature stabilises at 1400 K. At atmospheric pressure, nanodiamond graphitizes between 940 K and 1070 K [48, 49]. Therefore, low absorption grade (850 K) or electronic grade (400 K) material might be required to reach the pressures required for proposals [1–9].

However, the actual final temperatures are likely to be lower than those given by (4), as we have used the upper-bounds of the absorption coefficients. Alternative calculations for the disspipation of heat through blackbody radiation [50] predict lower final temperatures of 900 K (see Supplementary Information). It is also likely that the absorption will differ at the nanoscale compared to the bulk. For a particle radius of 25 nm and $\mathrm{N_s^0}$ concentration of 100-160 ppb, there are likely to only be one or two $\mathrm{N_s^0}$ defects per nanodiamond. In this regime, the surface is probably a more significant source of absorption than the bulk. High vacuum is commonly used in high-temperature annealing of diamond to prevent the onset of graphitization, which may further extend

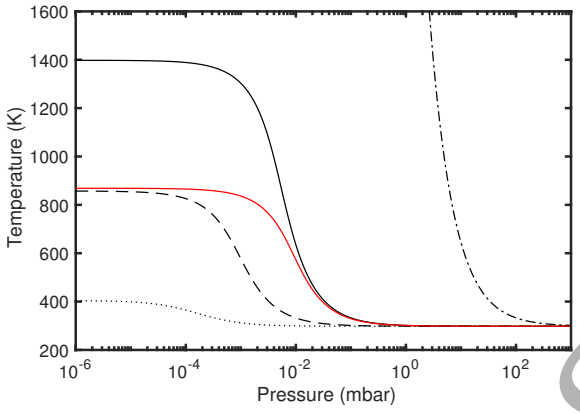


**Figure 4.** Modelled upper-bounds of temperature as a function of pressure for $r = 25$ nm nanoparticles and a trapping laser intensity of $I = 60$ GW/m$^2$ [14]. The absorption coefficient of the commercial nanodiamonds (— · —) used in [12–21] has been set to 30 cm$^{-1}$ based on 150 ppm $N_s^0$. Standard grade (——) corresponds to the bulk diamond grade used to make the nanodiamonds used in this study, with an upper-bound absorption coefficient 0.03 cm$^{-1}$. Low absorption grade (- - - -) has 0.003 cm$^{-1}$ [28, 29]. Electronic grade (·····) has a predicted absorption coefficient of $4.5 \times 10^{-5}$ cm$^{-1}$. The red line is a simulation of high purity silica with an absorption coefficient of 0.11 cm$^{-1}$ [38].

the level of attainable vacuum [51]. Since nanodiamonds are non-spherical (figure 2 (b)), they have a higher surface area-to-volume ratio, which assists gas cooling. It should also be noted that a previous study has shown that the spin coherence lifetime of the NV$^-$ centre ($T_2^*$) can be over 1 $\mu$s even for temperatures above 600 K [22]. Furthermore, the gas cooling term in (4) is known to underestimate heat dissipation away from thermal equilibrium [43].

Although we were unable to measure the temperature at the loss pressure, the simulation shows that heating would be limited to $< 10$ K above room temperature at 1 mbar (using the highest intensities and particle radius), which would suggest a different loss mechanism to the one proposed in [30] involving radiometric forces arising from temperature gradients across 3 $\mu$m silica spheres. The large thermal conductivity of diamond also would likely preclude the presence of temperature gradients. Rather, the smaller damping coefficient at lower pressure, combined with nonconservative scattering forces [52, 53], also proposed in [30], and shot-noise from the gas, are the more probable culprits in this trapping regime.

## 6. Conclusion

We have milled pure CVD diamonds into nanodiamonds and measured their resulting centre-of-mass motion in an optical dipole trap, from which we infer that the nanodiamonds do not heat up at 2-4 mbar. We attribute the previously observed heating in commercial nanodiamonds to the high concentration of bulk impurities. We have therefore demonstrated a route to levitating nanodiamonds in high vacuum and

have set upper-bounds on the temperatures they would reach by modelling the optical absorption of trapping light, and heat dissipation due to gas molecule collisions and blackbody radiation. This advance removes an obstacle that was preventing progress in using levitated nanodiamonds for probing quantum gravity, dark matter detection, phonon mediated coupling of electron spins, and mesoscopic wavefunction collapse.

## Acknowledgments

We acknowledge the EPSRC grants EP/J014664/1 and EP/J500045/1, and the European Union Seventh Framework Programme (FP7/2007-2013) under grant agreement no. 618078. G.W.M. is supported by the Royal Society. We are thankful to Ben Breeze for assistance with EPR, and to James Millen, James Bateman, and Darrick Chang for comments that improved the manuscript.

## References

[1] A. Albrecht, A. Retzker, and M. B. Plenio, Phys. Rev. A **90**, 033834 (2014).

[2] S. Bose, A. Mazumdar, G. W. Morley, H. Ulbricht, M. Toroš, M. Paternostro, A. Geraci, P. Barker, M. S. Kim, and G. Milburn, Phys. Rev. Lett. **119**, 240401 (2017).

[3] M. Scala, M. S. Kim, G. W. Morley, P. F. Barker, and S. Bose, Phys. Rev. Lett. **111**, 180403 (2013).

[4] Z. Q. Yin, T. Li, X. Zhang, and L. M. Duan, Phys. Rev. A **88**, 033614 (2013).

[5] C. Wan, M. Scala, S. Bose, A. C. Frangeskou, A. T. M. A. Rahman, G. W. Morley, P. F. Barker, and M. S. Kim, Phys. Rev. A **93**, 043852 (2016).

[6] C. Wan, M. Scala, G. W. Morley, A. T. M. A. Rahman, H. Ulbricht, J. Bateman, P. F. Baker, S. Bose, and M. S. Kim, Phys. Rev. Lett. **117**, 143003 (2016).

[7] A. Albrecht, A. Retzker, F. Jelezko, and M. B. Plenio, New J. Phys. **15**, 083014 (2013).

[8] C. J. Riedel, Phys. Rev. D **88**, 116005 (2013).

[9] C. J. Riedel and I. Yavin, Phys. Rev. D **96**, 023007 (2017).

[10] J. Wrachtrup and F. Jelezko, J. Phys. Condens. Matter **18**, S807 (2006).

[11] M. W. Doherty, N. B. Manson, P. Delaney, F. Jelezko, J. Wrachtrup, and L. C. L. Hollenberg, Phys. Rep. **528**, 1 (2013).

[12] L. P. Neukirch, R. Quidant, L. Novotny, and N. A. Vamivakas, Opt. Lett. **38**, 2976 (2013).

[13] L. P. Neukirch, E. von Haartman, J. M. Rosenholm, and N. A. Vamivakas, Nat. Photonics **9**, 653 (2015).

[14] T. M. Hoang, J. Ahn, J. Bang, and T. Li, Nat. Commun. **7**, 12250 (2016).

[15] R. M. Pettit, L. P. Neukirch, Y. Zhang, and N. A. Vamivakas, J. Opt. Soc. Am. B **34**, 31 (2017).

[16] T. M. Hoang, Y. Ma, J. Ahn, J. Bang, F. Robicheaux, Z.-Q. Yin, and T. Li, Phys. Rev. Lett. **117**, 123604 (2016).

[17] A. Kuhlicke, A. W. Schell, J. Zoll, and O. Benson, Appl. Phys. Lett. **105**, 073101 (2014).

[18] T. Delord, L. Nicolas, L. Schwab, and G. Hétet, New J. Phys. **19**, 033031 (2017).

[19] T. Delord, L. Nicolas, M. Bodini, and G. Hetet, Appl. Phys. Lett. **111**, 013101 (2017).

[20] J.-F. Hsu, P. Ji, C. W. Lewandowski, and B. D'Urso, Sci. Rep. **6**, 30125 (2016).

[21] A. T. M. A. Rahman, A. C. Frangeskou, M. S. Kim, S. Bose, G. W. Morley, and P. F. Barker, Sci. Rep. **6**, 21633 (2016).

[22] D. M. Toyli, D. J. Christle, A. Alkauskas, B. B. Buckley, C. G. Van de Walle, and D. D. Awschalom, Phys. Rev. X **2**, 031001 (2012).

[23] H. S. Knowles, D. M. Kara, and M. Atatüre, Nat. Mater. **13**, 21 (2014).

[24] M. E. Trusheim, L. Li, A. Laraoui, E. H. Chen, H. Bakhru, T. Schröder, O. Gaathon, C. A. Meriles, and D. Englund, Nano Lett. **14**, 32 (2013).

[25] E. J. G. Peterman, F. Gittes, and C. F. Schmidt, Biophys. J. **84**, 1308 (2003).

[26] J. Millen, T. Deesuwan, P. F. Barker, and J. Anders, Nat. Nanotechnol. **9**, 425 (2014).

[27] H. B. Dyer, F. A. Raal, L. Du Preez, and J. H. N. Loubser, Philos. Mag. **11**, 763 (1965).

[28] A. M. Bennett, B. J. Wickham, H. K. Dhillon, Y. Chen, S. Webster, G. Turri, and M. Bass, SPIE Photonics West 2014-LASE Lasers Sources **8959**, 89590R (2014).

[29] S. Webster, Y. Chen, G. Turri, A. M. Bennett, B. Wickham, and M. Bass, J. Opt. Soc. Am. B **32**, 479 (2015).

[30] G. Ranjit, D. P. Atherton, J. H. Stutz, M. Cunningham, and A. A. Geraci, Phys. Rev. A **91**, 051805 (2015).

[31] P. Mestres, J. Berthelot, M. Spasenovic, J. Gieseler, L. Novotny, and R. Quidant, Appl. Phys. Lett. **107**, 151102 (2015).

[32] J. Gieseler, B. Deutsch, R. Quidant, and L. Novotny, Phys. Rev. Lett. **109**, 103603 (2012).

[33] J. Gieseler, L. Novotny, and R. Quidant, Nat. Phys. **9**, 806 (2013).

[34] L. Novotny and B. Hecht, *Principles of Nano-Optics*, 2nd ed. (Cambridge University Press, 2012).

[35] G. Eaton, S. Eaton, D. Barr, and R. Weber, *Quantitative EPR*, 1st ed. (2010).

[36] J. Hees, A. Kriele, and O. A. Williams, Chem. Phys. Lett. **509**, 12 (2011).

[37] A. T. M. A. Rahman, A. C. Frangeskou, P. F. Barker, and G. W. Morley, arXiv:1710.01159 .

[38] R. Kitamura, L. Pilon, and M. Jonasz, Appl. Opt. **46**, 8118 (2007).

[39] T. Li, S. Kheifets, and M. G. Raizen, Nat. Phys. **7**, 527 (2011).

[40] V. Jain, J. Gieseler, C. Moritz, C. Dellago, R. Quidant, and L. Novotny, Phys. Rev. Lett. **116**, 243601 (2016).

[41] J. Vovrosh, M. Rashid, D. Hempston, J. Bateman, and H. Ulbricht, J. Opt. Soc. Am. B **34**, 1421 (2017).

[42] C. F. Bohren and D. R. Huffman, *Absorption and Scattering of Light by Small Particles*, Vol. 16 (Wiley, 1998).

[43] F. Liu, K. J. Daun, D. R. Snelling, and G. J. Smallwood, Appl. Phys. B Lasers Opt. **83**, 355 (2006).

[44] D. E. Chang, C. A. Regal, S. B. Papp, D. J. Wilson, J. Ye, O. Painter, H. J. Kimble, and P. Zoller, Proc. Natl. Acad. Sci. U. S. A. **107**, 1005 (2010).

[45] J. Walker, Reports Prog. Phys. **42**, 1605 (1979).

[46] R. P. Mildren and J. R. Rabeau, *Optical Engineering of Diamond*, 1st ed. (Wiley, 2013).

[47] D. T. Morelli and C. Uher, Appl. Phys. Lett. **63**, 165 (1993).

[48] J. Chen, S. Z. Deng, J. Chen, Z. X. Yu, and N. S. Xu, Appl. Phys. Lett. **74**, 3651 (1999).

[49] N. S. Xu, J. Chen, and S. Z. Deng, Diam. Relat. Mater. **11**, 249 (2002).

[50] J. Bateman, S. Nimmrichter, K. Hornberger, and H. Ulbricht, Nat. Commun. **5**, 4788 (2014).

[51] Y. Chu, N. D. Leon, B. Shields, B. J. M. Hausmann, R. Evans, M. J. Burek, M. Markham, A. Stacey, A. Zibrov, D. Twitchen, M. Loncar, H. Park, P. Maletinsky, and M. D. Lukin, Nano Lett. **14**, 1982 (2014).

[52] Y. Roichman, B. Sun, A. Stolarski, and D. G. Grier, Phys. Rev. Lett. **101**, 128301 (2008).

[53] P. Wu, R. Huang, C. Tischer, A. Jonas, and E. L. Florin, Phys. Rev. Lett. **103**, 108101 (2009).